Digital Beamforming for Near-Space Wide-Swath SAR Imaging

†‡§Wen-Qin Wang*, †Qicong Peng, †Jingye Cai
† School of Communication and Information Engineering,
University of Electronic Science and Technology of China, Chengdu, China, 610054
‡ Key Laboratory of Ocean Circulation and Waves, Chinese Academy of Sciences, 266071
§ Beijing Key Lab of Spatial Information Integration and 3S Engineering Applications, Peking University, 100871
*Email: wqwang@uestc.edu.cn; china_wqwang@hotmail.com

***Abstract*— Inspired by recent advances in near-space technology and synthetic aperture radar (SAR) technique, this paper presents one digital beamforming-based near-space wide-swath imaging technique. Near-space defined as the space region between $20km$ and $100km$, which is above storms and not constrained by orbital mechanics like satellite or high fuel consumption like airplane. These advantages make many new capabilities that are not accessible to current spacebore or airborne SAR being possible for near-space SAR. This also offers an opportunity to design new SAR imaging technique. This paper deals with conceptual design, as opposed to technological implementation. Multiple beams in azimuth are used to suppress the possible azimuth ambiguities for near-space high-resolution and wide-swath SAR imaging. An example near-space wide-swath SAR is conceptually designed. Simulation results show that the combination of digital beamforming technology and near-space platform can provide a promising solution for remote sensing applications.**

I. Introduction

Near-space, defined as the region between $20km$ and $100km$ [1], offers many capabilities that are not accessible for low earth orbit (LEO) satellites or airplanes. Once we step back from platform-based thinking and look at the effects, near-space will be of great interest because it provides new remote sensing opportunities. Near-space platform offers two obvious advantages [2]: Firstly, it is above the troposphere and atmosphere region where most weather occurs, so a high velocity can be achieved. Secondly, it is low cost. Near-space platform inherent simplicity, recoverability, and without space-hardening requirements all contribute to this strong advantage. Moreover, if the payloads they carried have malfunction, they can be brought back and repaired. Thus, by placing radar sensors into near-space, many functions that are currently performed with satellites or airplanes could be performed much more cheaply [3].

On the other hand, future SAR will be required to produce high-resolution imagery over a wide area of surveillance. However, minimum antenna area constraint makes it a contradiction to simultaneously obtain both unambiguous high azimuth resolution and wide-swath. Consequently, current spaceborne SAR has an imaging capability of wide-swath but with a limited azimuth resolution. In contrast, airborne SAR has an imaging capability of high-resolution but with a limited swath coverage. There is therefore a clear incentive consideration to increase swath coverage and azimuth resolution simultaneously. As near-space aircraft can operate in the altitude higher than that of an airplane but lower than that of a satellite, and can fly with a velocity as fast as $1500m/s$; hence the requirement for simultaneous high-resolution and wide-swath SAR imaging is more easier to be satisfied for near-space platform than both satellite and airplane platforms.

This paper presents one digital beamforming-based near-space wideswath imaging technique. Multiple beams in azimuth are used to suppress the possible azimuth ambiguities for near-space high-resolution and wide-swath (HRWS) SAR imaging, and deals with conceptual design, as opposed to technical implementation. The focus is placed on presenting new concepts, system model and performance analysis. The remaining sections are organized as follows. Section II conceptually designs digital beamforming-based near-space HRWS SAR imaging, followed by ambiguity analysis in Section III. Section IV investigates the performance of an example near-space HRWS SAR system. This paper is concluded in Section V.

II. Conceptual Design

The design of near-space SAR involves a wide range of sometimes conflicting requirements on coverage, spatial resolution, revisit access times. The illuminated swath must be restricted so that the received radar echoes are unambiguous in range or/and azimuth. As an example, assuming an X-band near-space SAR system with the following typical parameters: wavelength is $\lambda = 0.03m$, incidence angle is $\eta = 60°$, flying velocity is $v_s = 1000m/s$, antenna length is $L_a = 0.4m$, antenna width is $H_a = 0.22m$, and flying altitude is $H_0 = 60km$, then the maximal swath width is W_s is find to be $32.7km$. Thus the unambiguous swath width and the achievable azimuth resolution still pose tough requirements on near-space SAR system design. Moreover, the attainment of wide-swath will become increasingly difficult if higher spatial resolution is required, due to the requirement of increased PRF. The PRF limit for a certain swath W_s and a given incidence angle η is [4]

$$\frac{2v_s}{L_a} \le PRF \le 0.8\frac{c_0}{2W_s \sin(\eta)}. \quad (1)$$

978-1-4244-2193-0/08/$25.00 ©2008 IEEE

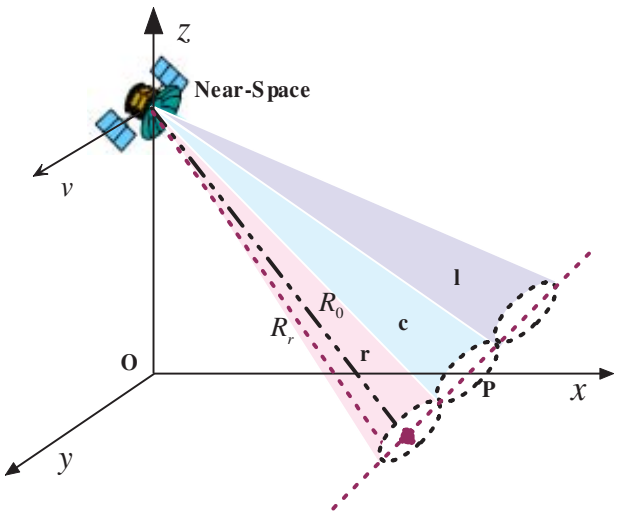

Fig. 1: Model of near-space SAR for high-resolution and wide-swath imaging.

To overcome the inherent limitations of conventional SAR to perform HRWS imaging, this paper uses multiple (e.g. N) beams in azimuth, as shown in Fig. 1. This arrangement enables correct sampling of the azimuth spectrum with a PRF fitting the total antenna azimuth length, which is N times smaller than the PRF necessary for the antenna azimuth length L_a.

Then, the area of each beam antenna is restricted by

$$A_{as} \geq \frac{4v_s\lambda R_c \tan(\eta)}{c_0} \cdot \frac{1}{N}. \tag{2}$$

Clearly the minimum area of each beam antenna is N-times smaller than the respective area of a monostatic SAR. By rearranging the terms in Eq. (2) using the expression for the azimuth resolution of SAR, the ratio of swath width to azimuth resolution is found to be

$$\frac{W_s}{\rho_a} \leq \frac{Nc_0}{2v_s \sin(\eta)}. \tag{3}$$

From Eq. (3) we can notice that the relation not only depends on the platform velocity v_s and the incidence angle η but also on the number of antenna beams. The ratio $c_0/2v_s$ is about 150 000 for near-space platforms, but nearly constant at 20 000 for LEO satellites and in the range of 300 000 to 750 000 for airplanes.

Thereafter, the displaced phase centre technique [5] can be used to gain additional samples along the the synthetic aperture which enables an efficient suppression of azimuth ambiguities, i.e., the multiple beams in azimuth allows for the division of a broad Doppler spectrum into multiple narrow-band subspectra with different Doppler centroids. A coherent combination of the subspectra will then yield a broad Doppler spectrum for high azimuth resolution. Thus this technique is hence especially attractive for high-resolution SAR that uses a long antenna for unambiguous wide-swath coverage.

As shown in Fig. 1, a distinct channel is associated with each beam signal which is separately amplified, down-converted and digitized. By this way, the acquired data are split according to the azimuth angular position, i.e., the instantaneous Doppler centre frequency. As a result, while given knowledge of the relative squint angles of each beam (and hence the Doppler centre frequency for each beam) and assuming suitable isolation between the beams, each channel can be sampled at the Nyquist rate appropriate to the bandwidth covered by each narrow beams, instead of that covered by the full beamwidth.

III. Ambiguity Analysis

For a given range and azimuth antenna pattern, the PRF must be selected such that the total ambiguity noise contribution is enough small relative to the signal, i.e., −18 to −20 dB. A low PRF will increase the azimuth ambiguity level due to increased aliasing of the azimuth spectra. On the other hand, a high PRF value will reduce the interpulse period and result in overlap between the received pulses in time. To solve this problem, the transmit interference restriction on the PRF must be satisfied with

$$\frac{n'}{\frac{2R_1}{c_0} - \tau_p - \tau_{RP}} < PRF < \frac{n'+1}{\frac{2R_N}{c_0} + \tau_{RP}} \tag{4}$$

where R_1 is the slant range to the first data sample, R_N is the slant range to the last (Nth) data sample in the recording window, n' is a given integer, and τ_{RP} is the receiver protect window extension about the pulse duration τ_p.

Similarly, the nadir interference restriction on the PRF can be represented by

$$\frac{m'}{\frac{2R_1}{c_0} - 2\tau_p - \frac{2H_0}{c_0}} < PRF < \frac{m'}{\frac{2R_N}{c} - \frac{2H_0}{c_0}} \tag{5}$$

where m' is a given integer. As supposed previously, $H_0 = 60km$, then the partial unambiguous PRF zones defined by Eqs. (4) and (5) is illustrates in Fig. 2.

Alternatively, given a PRF or range of PRFs as shown in Fig. 2, the antenna dimensions and/or weighting (to lower the sidelobe energy) must be applied such that the ambiguity-to-signal ratio specification is met. The azimuth ambiguities arise from finite sampling of the Doppler spectrum at intervals of the PRF. Since the azimuth spectrum repeats at PRF intervals, the signal components outside this frequency interval will fold back into the main part of the spectrum, and the desired signal band will be contaminated by the ambiguous signals from adjacent spectra. This can be evaluated by the azimuth ambiguity to signal ratio (AASR) defined as [6]

$$AASR \approx \frac{\sum_{\substack{m=-\infty \\ m\neq 0}}^{\infty} \int_{-0.5B_d}^{0.5B_d} G^2(f + m \cdot PRF)df}{\int_{-0.5B_d}^{0.5B_d} G^2(f)df} \tag{6}$$

where B_d and $G(f)$ denote the SAR correlator azimuth processing bandwidth and the azimuth antenna pattern, respectively.

Considering the three beams illustrated in Fig. 1, we have

$$G_k(\theta) = sinc^2\left(\frac{\pi L_{as}\cos(i\cdot\theta_s)}{\lambda}\sin(\theta - i\cdot\theta_s)\right), \quad i \in (-1, 0, 1) \tag{7}$$

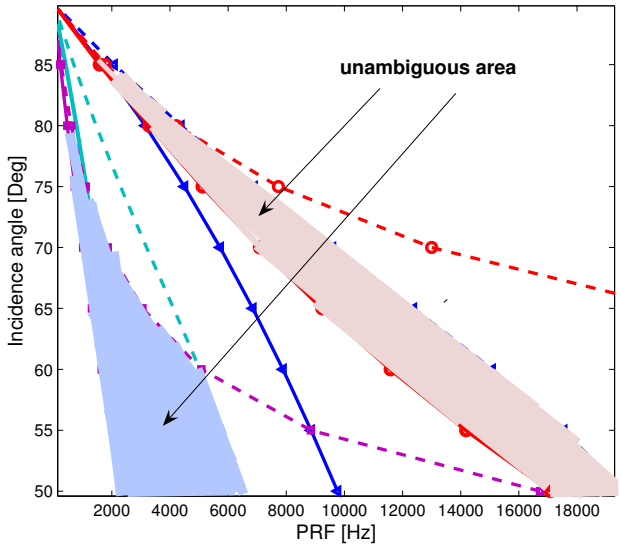

Fig. 2: Plot of partial azimuth unambiguous area against incidence angle.

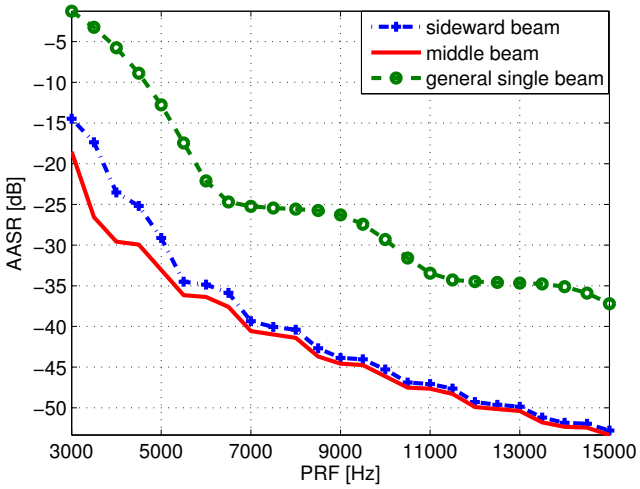

Fig. 3: The AASR of an example near-space SAR as a function of PRF.

Note that $i \in (-1, 0, 1)$ is accordingly determined from the positions of the three beams, i.e., $i = -1$ is for the left beam, $i = 0$ is for the central beam and $i = 1$ is for the right beam. Because the $3dB$ beam-width is approximately determined by [6]

$$\theta \approx \frac{\lambda}{2v_s} f, \qquad \theta_s = k_a \frac{\lambda}{L_{as}} \tag{8}$$

with k_a a given constant. Eq. (7) can then be further simplified into

$$G_k(f) \approx sinc^2[\pi L_{as} \cos(i \cdot \frac{k_a c_0}{f L_{as}})(\frac{f}{2v_s} - i \cdot \frac{k_a}{L_{as}})], \quad i \in (-1, 0, 1) \tag{9}$$

Then, from Eq. (6) we can get

$$\begin{aligned} AASR_i(PRF) = \{ \sum_{\substack{m=-\infty \\ m\neq 0}}^{\infty} [& \int_{(i-0.5)B_{ds}}^{(i+0.5)B_{ds}} G_i^2(f + m \cdot PRF) df \\ & + \sum_{j \neq i} \int_{(i-0.5)B_{ds}}^{(i+0.5)B_{ds}} G_i(f + m \cdot PRF) G_j(f + m \cdot PRF) df] \} \\ & \cdot \{ \int_{(i-0.5)B_{ds}}^{(i+0.5)B_{ds}} G_i^2(f) df + \sum_{j \neq i} \int_{(i-0.5)B_{ds}}^{(i+0.5)B_{ds}} G_i(f) G_j(f) df \}^{-1}, \\ & i, j \in (-1, 0, 1) \end{aligned} \tag{10}$$

To manifest the results of AASR an example near-space SAR is considered with the following parameters: $H_0 = 60km$, $v_s = 1000m/s$, $\lambda = 0.03m$, $L_{as} = 1.2m$, then the AASR can be illustrated as Fig. 5. Notice that, the AASR is typically specified to be on the order of $-20dB$; however, even at this value ambiguous signals can be observed in images that have very bright targets adjacent to dark targets, because SAR imagery can have an extremely wide dynamic range due to the correlation compression gain. As such, a lower AASR, e.g., $-30dB$, is desirable.

Similarly, range ambiguities may result from preceding and succeeding pulse echoes arriving at the antenna simultaneously with the desired return. This type of ambiguity is relatively not significant for near-space SAR. The range ambiguity of the near-space HRWS SAR discussed in this paper can be analyzed in a like manner as the general SAR, which has been fully investigated [7].

Thus the set of PRFs is therefore established by the maximum acceptable range and azimuth ambiguity-to-signal ratios, as well as the transmit and nadir interference. Notice that, there may be no acceptable PRFs at some incidence angles that meet the minimum requirements. The designer then has the option to relax the performance specifications for these imaging areas or exclude these modes from the operations plan, e.g., multi-beam in azimuth and/or range direction as discussed in this paper.

IV. Performance of an Example System

A quantity directly related to SAR processing is the noise equivalent sigma zero (NESZ) defined as the radar cross section for which the SNR is equal to 1 ($SNR = 0\ dB$). The NESZ can also be interpreted as the smallest target cross section which is detectable by the SAR system against thermal noise. From the radar equation [8] we can get [9]

$$NESZ = \frac{8\pi R_s^3 v_s \lambda K T_{sys} F L_f}{P_{avg} N A_{as}^2 \rho_r} \tag{11}$$

where R_s is the slant range which can be assumed constant, K ($K \approx 1.38 \times 10^{-23}$) the Boltzmann constant, T_{sys} the system noise temperature, L_f the loss factor, F the receiver noise figure, P_{avg} the average transmit power and ρ_r the size of the range resolution cell for one look.

To further evaluate the quantitative performance of near-space HRWS SAR an example system is considered. The

Table I: Performance parameters of an example near-space HRSW SAR.

Parameters	Variables	Values
mean transmit power	P_{avg}	$10W$
number of antenna subarrays	N	3
transmit/receive antenna length	L_{as}	$1.2m$
near-space platform velocity	v_s	$1000m/s$
incidence angle	η	$70°$
antenna width	H_a	$0.2m$ (minimum 0.16m)
swath width	W_s	$76.94km$
sub-beam azimuth width	θ_s	$8.59°$
radiometric resolution	$NESZ$	$-37.11dB$
incidence angle	η	$75°$
antenna width	H_a	$0.33m$ (minimum 0.29m)
swath width	W_s	$81.43km$
sub-beam azimuth width	θ_s	$5.21°$
radiometric resolution	$NESZ$	$-37.83dB$
incidence angle	η	$80°$
antenna width	H_a	$0.7m$ (minimum 0.65m)
swath width	W_s	$85.28km$
sub-beam azimuth width	θ_s	$2.46°$
radiometric resolution	$NESZ$	$-39.16dB$

SAR operates in X-band with a center frequency of 10GHz. The geometric ground-range and azimuth resolution are set to $\rho_r = 0.2m$ and $\rho_a = 0.2m$, respectively. To calculate the system performance, an overall loss factor $L_f = 3\ dB$, a fixed flying height of $60km$, and a receiver noise figure of $F = 3\ dB$ are assumed. It is further assumed that the signal bandwidth is adjusted for varying incidence angle such that the ground-range resolution is constant across the swath. The swath width is calculated from Eq. (3). The system performance is represented by the radiometric resolution of the SAR image given by the NESZ in Eq. (11). One example system design is provided in Table I. We can notice that, for the incidence angle given in Table I the swath of the near-space HRSW SAR ranges from $75-85\ km$ and the NESZ is approximately $-37dB$. These results show that a satisfied performance can be achieved, however with only a small number of antenna beams, and a total antenna size not larger than that of current systems.

An important conclusion is the unambiguous range and swath width can be further increased by using a near-space SAR with multiple beams in azimuth. But, since a drawback to multiple beams is the need for interbeam suppression, some additional means of interbeam suppression should be provided to make the system viable. One possible technique is the use of waveform diversity to provide some cross-cancellation of data in different channels [10]. This will be treated in subsequent paper. Another disadvantage of near-space maneuvering vehicles as sensor platforms is the limited payload weight.

V. Conclusion

Near-space offers a significant new remote sensing opportunity and is a key remote sensing resource. Inspired by recent advances in near-space technology, this paper proposes firstly the concept of near-space SAR for HRWS SAR imaging. The novelty resides in the sensor platform. It is shown that, the use of cost effective near-space platforms can lead to the solutions that previously thought to be out of reach for remote sensing and government customers [11]. However, there are several technical challenges [12]. The first technological challenge is motion compensation. As a matter of fact, problems arise due to the presence of atmospheric turbulence, which introduce the trajectory deviations from the normal position, as well as altitude (roll, pitch, and yaw angles) [13]. For current SAR systems, the motion compensation is usually achieved with GPS (Global Position Systems) and INU (Inertial Navigation Units). However, for near-space SAR the motion measurement facilities may be not reachable, so some new efficient motion compensation algorithms must be developed. We think the raw data based autofocus algorithms may be the best choice. We plan to carry out further investigation in these problems during subsequent work. Although achieving the potential of near-space SAR for remote sensing applications will require significant work and progress on many fronts, we are indeed convinced the effort will be worth it.

ACKNOWLEDGEMENTS

This work was supported in part by the Open Fund of the Key Laboratory of Ocean Circulation and Waves, Chinese Academy of Sciences under Contract number *KLOCAW0809*; and supported in part by the Open Fund of the Beijing Key Lab of Spatial Information Integration and 3S Application, Peking University under Contract number *SIIBKL08-1-04*.

References

[1] E. B. Tomme, "Balloons in today's military: an introduction to the near-space concept," *Air Space. J.*, 2005, vol. 19, no. 4, pp. 39–50.

[2] W. Q. Wang, "Application of near-space passive radar for homeland security," *Sens. Imag.: An Int. J.*, 2007, vol. 8, no. 1, pp. 39–52.

[3] W. Q. Wang, J. Y. Cai, and Q. C. Peng, "Near-space SAR: a revolutionizing remote sensing mission," Proc. of *Asia-Pacific Synthetic Aperture Radar Conf.*, Huangshan, China, 2007, pp. 127–131.

[4] A. Currie, and M. A. Brown,, "Wide-swath SAR," *IEE Proc. Radar Sonar Navig.*, 1992, vol. 139, no. 2, pp. 122–135.

[5] A. Bellettini, and M. A. Pinto, "Theoretical accuracy of synthetic aperture sonar micronavigation using a displaced phase-center antenna," *IEEE J. of Oceanic Engineering*, 2002, vol. 27, no. 4, pp. 780–789.

[6] F. K. Li, and W. T. K. Johnson, "Ambiguities in spaceborne synthetic aperture radar systems," *IEEE Trans. Aerosp. Electron. Syst.*, 1983, vol. 19, no. 3, pp. 389–397.

[7] J. C. Curlander, and R. N. McDonough, *Synthetic Aperture Radar: Systems and Signal Processing*, John Wiley& Sons, Inc, New York, USA, 1991.

[8] D. R. Wehner, *High Resolution Radar*, Artech House, Norwood, MA, 2nd Edition.

[9] G. Krieger, and A. Moreira, "Spaceborne bi- and multistatic SAR: potential and challenges," *IEE Proc. Radar Sonar Navig.*, 2006, vol. 153, no. 3, pp. 184–198.

[10] P. A. Zulch, R. H. Hancock, W. Moran, S. Suvorova, and J. Byrnes, "Transmit waveform diversity for space based radar," Proc. of *IEEE Aerospace Conf.*, Big Sky, MT, USA, 2007.

[11] W. Q. Wang, "Near-Space Passive Remote Sensing for Homeland Security: Potential and Challenges," Proc. *XXI Int. Society for Photogrammetry Remote Sens.*, Beijing, Jul. 2008, pp. 1021–1027.

[12] W. Q. Wang, "Approach of adaptive synchronization for bistatic SAR real-time imaging," *IEEE Trans. Geosci. Remote Sens.*, 2007, vol. 45, no. 9, pp. 2695–2700.

[13] G. Fornaro, G. Franceschetti, and S. Pema, "Motion compensation errors: effects on the accuracy of airborne SAR images," *IEEE Trans. Aerosp. Electron. Syst.*, 2005, vol. 41, no. 4, pp. 1338–1351.